Metrics for Evaluation and Design of Large-Displacement Linear-Motion Compliant Mechanisms

Article *in* Journal of Mechanical Design · January 2012

DOI: 10.1115/1.4004191

CITATIONS
29

READS
715

5 authors, including:

Spencer P. Magleby
Brigham Young University - Provo Main Campus
269 PUBLICATIONS **6,287** CITATIONS
SEE PROFILE

David Smith
ALPINE ENGINEERING & DESIGNS, INC
4 PUBLICATIONS **35** CITATIONS
SEE PROFILE

Larry L. Howell
Brigham Young University - Provo Main Campus
425 PUBLICATIONS **9,816** CITATIONS
SEE PROFILE

Brian D. Jensen
Brigham Young University - Provo Main Campus
151 PUBLICATIONS **2,280** CITATIONS
SEE PROFILE

Allen B. Mackay
Medical Products Division,
W. L. Gore and Associates,
Flagstaff, AZ 86001
e-mail: allen.mackay@byu.net

David G. Smith
Compliant Mechanism Research,
Brigham Young University,
Provo, UT 84602
e-mail: david.gar.smith@gmail.com

Spencer P. Magleby[1]
e-mail: magleby@byu.edu

Brian D. Jensen
e-mail: bdjensen@et.byu.edu

Larry L. Howell
e-mail: lhowell@byu.edu

Department of Mechanical Engineering,
Brigham Young University,
Provo, UT 84602

Metrics for Evaluation and Design of Large-Displacement Linear-Motion Compliant Mechanisms

This work introduces metrics for large-displacement linear-motion compliant mechanisms (LLCMs) that evaluate the performance tradeoff between displacement and off-axis stiffness. These metrics are nondimensionalized, consisting of relevant characteristics used to describe displacement, off-axis stiffness, actuation force, and size. Displacement is normalized by the footprint of the device, transverse stiffness by a new performance characteristic called virtual axial stiffness, and torsional stiffness by the characteristic torque. These metrics account for the variation of both axial and off-axis stiffness over the range of displacement. The metrics are demonstrated for several microelectromechanical systems (MEMS) that are sensitive to size because of high cost and off-axis stiffness because of function. The use of metrics in design is demonstrated in the design of an LLCM; the resulting design shows increased values for both the travel and transverse-stiffness metrics. [DOI: 10.1115/1.4004191]

Keywords: linear-motion metrics, stiffness, compliant mechanisms, linear motion, microelectromechanical systems, off-axis stiffness

1 Introduction

Recent maturation in methods for modeling and designing compliant mechanisms has spurred their use in a variety of applications. Compliant mechanisms offer some advantages over rigid mechanisms; however, compliant mechanisms are faced with their own challenges that require further development. One particularly elusive aspect is the development of large-displacement linear-motion mechanisms with high off-axis stiffness.

While linear motion is attractive for many applications, mechanisms with large linear displacement generally employ sliding surfaces (prismatic joints) to constrain the device to one degree of freedom. Traditional linear-motion mechanisms that use prismatic joints are compact and provide a long range of motion relative to their size. However, prismatic joints have inherent challenges related to lubrication, friction, and wear. Due to the clearance in the joint, prismatic joints also often suffer from backlash unless they are preloaded or manufactured to high tolerances. This has led engineers to seek alternatives to prismatic joints for some applications that require linear motion.

Compliant mechanisms could offer an alternative to traditional linear-motion mechanisms both in terms of improved functionality and decreased cost. Because compliant mechanisms gain some or all of their motion from deflection of the parts [1], they have the potential to completely eliminate relative motion between linkage interfaces (joint surfaces) and thus eliminate friction in the joints. As an added benefit, because compliant members couple energy storage with motion, stable positions can be integrated into the design [2].

Several linear-motion compliant mechanisms, including bistable mechanisms, have been developed. They are usually employed in mechanisms that require only small displacements, such as micro-relays. Compliant mechanisms that have a longer range of travel often have significantly reduced off-axis stiffness due to the use of long flexural members. Most existing linear-motion compliant mechanisms either produce long travel with low off-axis stiffness or exhibit high off-axis stiffness over a short range of travel.

The development of well-defined performance metrics adapted to the more sophisticated performance characteristics of large displacement systems could be a useful aid to designers considering their use. These metrics would allow for the comparative evaluation of various configurations and the optimization of particular configurations.

The objective of this paper is to provide metrics for evaluating the performance of large-displacement linear-motion compliant mechanisms (LLCMs) to demonstrate the metrics on various LLCMs and to illustrate their use in the comparison of LLCMs. The paper will focus on the in-plane performance of linear mechanisms.

2 Attributes of Linear Motion Mechanisms

Off-axis stiffness, or the propensity for a mechanism to resist motion in unwanted directions, is an important consideration for large-displacement compliant mechanisms [3]. Linear-motion mechanisms generally consist of a support structure that guides a portion of the mechanism (called the "shuttle") in linear translation. Several examples are shown in Fig. 1. Previous studies in linear-motion compliant mechanisms have usually focused on mechanisms with relatively small displacements. These mechanisms have been evaluated using metrics that evaluate performance at a single position, usually the default or "home" position. When considering larger displacements, it is essential to have metrics and design approaches that account for variability in key performance criteria throughout the entire range of displacement.

Effective LLCM designs should effectively guide the shuttle along the axis of travel, providing resistance to off-axis movement while allowing it to travel relatively freely in the axial direction. Several linear-motion compliant mechanisms have been developed with these behaviors. Some exhibit nearly linear force-deflection behavior along the axis of travel (such as the folded

[1]Corresponding author

Contributed by the Design Innovation and Devices Division of ASME for publication in the JOURNAL OF MECHANICAL DESIGN. Manuscript received August 18, 2009; final manuscript received March 29, 2011; published online January 4, 2012. Assoc. editor: Mary Frecker.

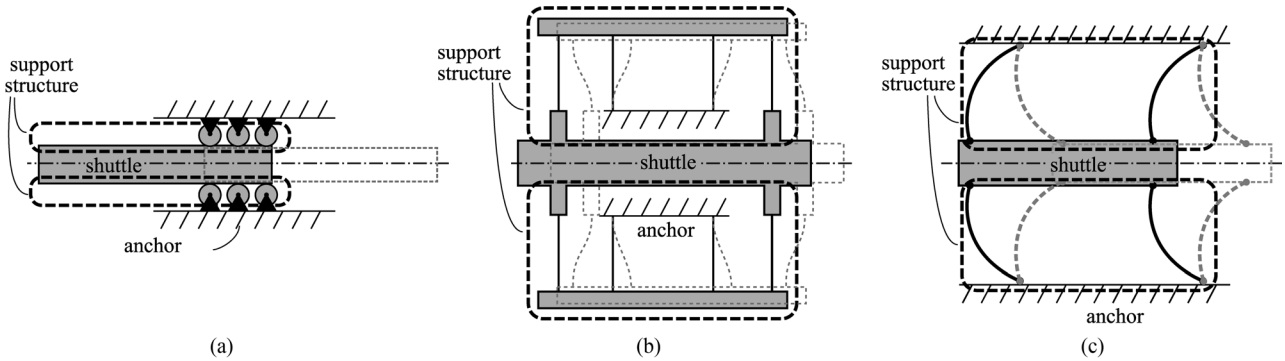

Fig. 1 Examples of linear-motion mechanisms: (*a*) rigid-body linear roller bearing; (*b*) compliant folded-beam mechanism; (*c*) compliant bistable mechanism

beam [4], the double V-beam [5], CT joint [3], and the XBob [6]), while others exhibit nonlinear, bistable force-deflection behavior (such as the LDBM [7–9], SRFBM [10], and the DTBM [11]). Travel, δ, and axial and transverse directions are defined for linear-motion mechanisms in Fig. 2.

Several studies have considered off-axis stiffness properties [3,4,8,12]. Off-axis stiffness for a LLCM has been defined as the ratio of the stiffness in an undesirable direction divided by the stiffness in the intended direction of motion [13]. Several mechanisms in prior work have sought to increase axial displacement while maintaining off-axis stiffness [3]. The compliant translational joint developed by Trease et al. [3] exhibited large linear displacement and a high stiffness ratio ($k_{transverse}$:k_{axial}) at the home position.

For large displacement mechanisms, it would be advantageous for the off-axis stiffness to be addressed along the entire range of travel. Off-axis stiffness is usually a function of axial displacement rather than a characteristic of the mechanism [4]. With this in mind, this work seeks to develop a set of performance metrics that accounts for off-axis stiffness across the entire range of axial travel for a given mechanism. Here we will define stiffness as the change in force required to take the next step in displacement ($\Delta F/\Delta x$). A more complete review of force and stiffness can be found in Ref. [14].

Resistance to motion in the undesired direction (off-axis stiffness) includes two key attributes: transverse stiffness, $k_{transv}(x)$, and torsional stiffness, $k_{tors}(x)$. These two attributes are functions of axial position as can be seen in Figs. 3 and 4. Because they are often nonconstant over the range of travel, it is imperative that representative values be taken from the critical values of the functions rather than relying on home position evaluations alone. The most critical values for these two functions are the minimum stiffness, $k_{transv,min}$ and $k_{tors,min}$, respectively. In this case, these values are at the yield stress limits shown on the graphs and correspond to the minimum stiffness.

The outcome of interest in the axial direction is the force required to actuate the mechanism. Hence it is the maximum axial force, $F_{ax,max}$, (and not the axial stiffness), which describes the critical resistance to motion in the axial direction. This actuation force is the maximum axial force over the range of travel. For a mechanism with a linear force-displacement relation, the actuation force corresponds to the force at maximum displacement (in this case defined by the yield stress), while with a bistable mechanism the actuation force is at an intermediate position. Misdirected actuation forces, which could be the source of transverse loads, are likely to be on the same order of magnitude as the actuation force. Thus this actuation force sets a global scale for the loads associated with the mechanism.

Other key attributes of LLCMs are the total displacement, δ, and the mechanism size, d. The key attributes are summarized in Table 1. In the following sections, these attributes will be combined to formulate nondimensional groups that function as suitable performance metrics.

3 Performance Metrics for LLCMs

The three aspects of performance that are measured with the proposed metrics include displacement, in-plane transverse stiffness, and in-plane torsional stiffness.

3.1 Criteria for Formulating Displacement and Stiffness Metrics. The ideal LLCM would have large displacement relative to its size. Therefore, a suitable metric for travel would

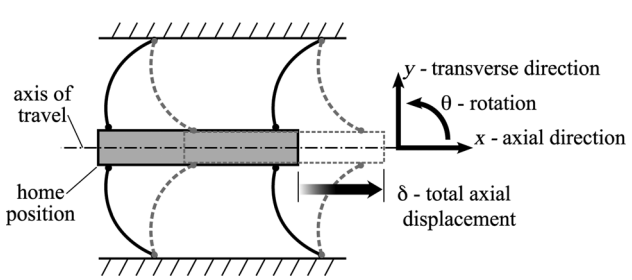

Fig. 2 Key definitions for a typical linear-motion compliant mechanism, including axial and transverse directions and total axial displacement

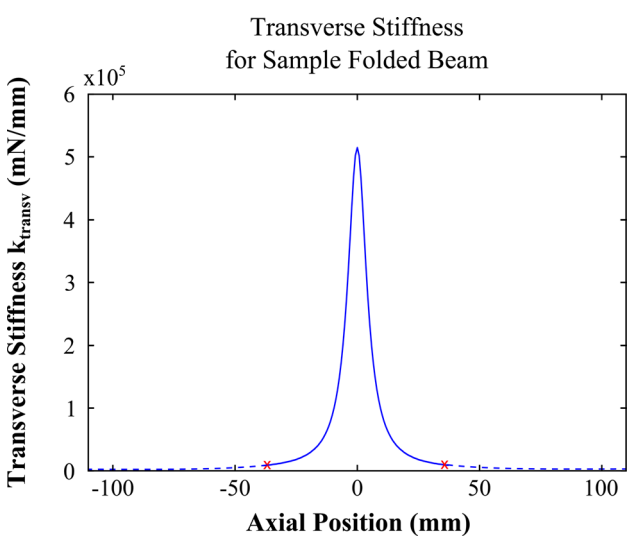

Fig. 3 The function of transverse stiffness over the range of axial displacement. The solid portion of the graph indicates axial positions within the yield strength of the material.

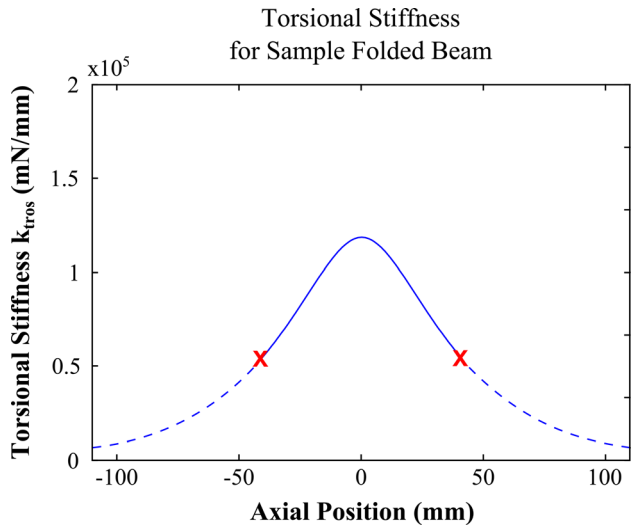

Fig. 4 The function of torsional stiffness over the range of axial displacement. The solid portion of the graph indicates axial positions within the yield strength of the material.

normalize the displacement of a device by its size or footprint. While measuring displacement is straightforward, the definition of the size of a mechanism is a topic to be considered. The discussion that follows seeks to define a characteristic length against which the displacement can be compared. This definition of "mechanism size" will have a large role in normalizing performance in displacement and off-axis stiffness.

In the formulation of off-axis stiffness and displacement metrics, there are several necessary features that will make the metrics effective in evaluating, normalizing, and comparing performance. First, the metric must consist of relevant attributes that describe the performance of the mechanism. In addition, the metric must consistently rate the performance of all the parameters. Finally, the metric should appropriately normalize the desired performance (e.g., off-axis stiffness by axial resistance) and result in a nondimensional parameter.

There are several other desirable attributes that would improve the utility of an off-axis stiffness metric. The metric should be able to deal with extremes in off-axis stiffness, such as instabilities in the off-axis direction. It should also include the option to plot the stiffness as a function of displacement and to characterize a worst-case stiffness. This need is illustrated with a sample of the off-axis stiffness functions for the folded beam mechanism is

Table 1 A list and description of the key attributes for LLCMs that will be used in the formulation of the performance metrics

Attribute Description	Critical Value	Variable Name	Bistable Example	Linear Example
Resistance to motion in the desired direction (x)	Maximum axial force	$F_{ax,max}$	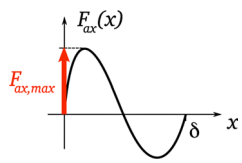	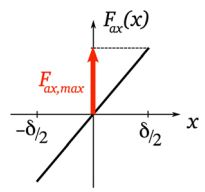
Resistance to motion in the transeverse direction (y)	Minimum transverse stiffness	$K_{transv,min}$	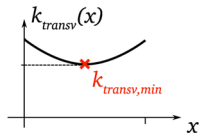	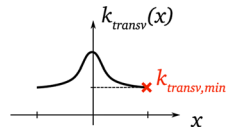
Resistance to rotation (θ)	Minimum torsional stiffness	$K_{tors,min}$	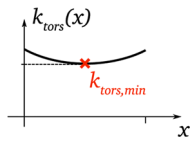	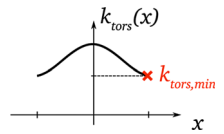
Total displacement in the desired direction	Displacement	δ	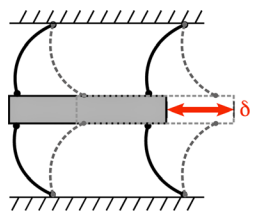	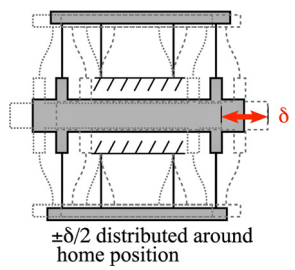
2-dimensional space requirement	Diagonal of bounding box	d	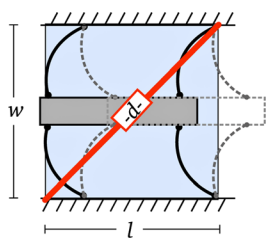	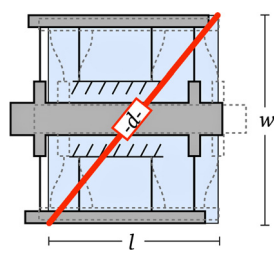

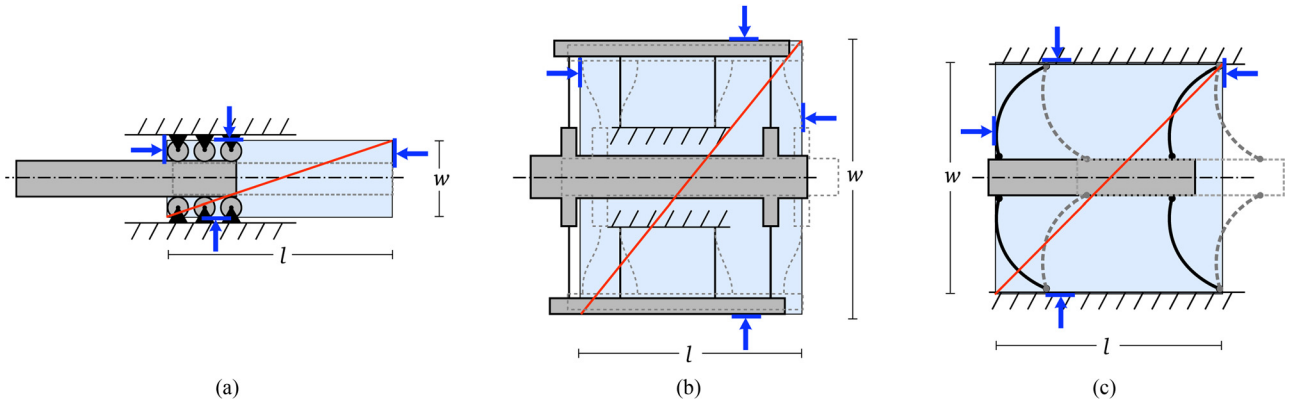

(a) (b) (c)

Fig. 5 The size of 2D linear mechanisms can be described by the bounding box defined by the widest and longest instances. The limiting features of the support structure are indicated by the arrows for these three cases.

shown in Figs. 3 and 4. Note the large change in stiffness as the folded-beam is deflected from its home position.

In other situations, it will be useful to quantify stiffness by reducing the stiffness function to a single representative value. This worst-case stiffness can be normalized by comparison to the axial resistance, distilling the mechanism performance to a single nondimensional number.

3.2 The Displacement Metric. Because of packaging considerations, it is generally desirable to create a compact mechanism while delivering the performance needed. For example, handheld devices that incorporate linear motion, such as devices with translating displays or keypads, require mechanisms that deliver large travel while requiring very little "real estate" within the device. The length and width dimensions of the footprint as indicated in Fig. 5, create a bounding box that encloses the mechanism in its widest and longest instances, including all motions during deflection. For example, for the folded beam suspension of Fig. 5(*b*), the mechanism is widest at its undeflected position and longest at its deflected position. Hence the bounding box uses the width of the undeflected mechanism and the length of the deflected mechanism. For Fig. 5(*c*), the length for the undeflected state and the deflected state are equal, and either could be used for the bounding box, but the bounding box should encompass one or the other and not both instances. The bounding box approach gives preference to compact mechanisms, but it does not limit the application of the metrics to known mechanisms. This opens the possibility of asymmetry or other unique configurations that could be developed in future mechanisms.

The bounding box is defined to include the width and length of the support structure and the portion of the shuttle that contributes to the linear motion as shown for the examples in Fig. 5. It does not include the anchor or extensions of the shuttle because these features are largely independent of mechanism performance. The width of the shuttle is included because torsional stiffness will depend largely upon mechanism size, both in width and length. These definitions of overall length and width suggest that the optimal size for a mechanism approaches $w=0$. The ideally sized linear mechanism would have a narrow support structure, approaching $w=0$ in the limit. The mechanism's support structure would also be short in the axial direction. However, unlike the width, the length of the bounding box has a nonzero limit, based on the total deflection, δ.

The length of the diagonal, d, is defined as

$$d = \sqrt{w^2 + l^2} \tag{1}$$

which combines the length and width into a single characteristic length by which the displacement can be normalized. The normalized displacement metric is then defined as

$$\delta^* = \frac{\delta}{\sqrt{w^2 + l^2}} \tag{2}$$

This formulation provides a metric, that is, consistent in its ratings, and correctly displays improvements in the travel, length, and width.

3.3 The Transverse Stiffness Metric. From the preceding discussions, it can be seen that the items of interest for the transverse and axial resistance are the transverse stiffness, k_{transv}, and the actuation force, $F_{ax,max}$. The mechanism displacement, δ, is employed to create the normalized transverse stiffness metric, k^*_{transv}, defined as

$$k^*_{transv} = \frac{k_{transv,min}}{F_{ax,max/\delta}} \tag{3}$$

This metric successfully integrates the required and desired qualities of an off-axis stiffness metric. It consists entirely of characteristic values. The ratio is unitless with the denominator resembling an overall stiffness in the axial direction. For this reason, the expression in the denominator is termed the virtual axial stiffness, $k_{ax,virt}$, where

$$k_{ax,virt} = \frac{F_{ax,max}}{\delta} \tag{4}$$

This interpretation of the metric is illustrated in Fig. 6. For a linear spring with constant stiffness, the virtual stiffness is exactly half the axial stiffness, as illustrated in Fig. 6(*b*).

3.4 The Torsional Stiffness Metric. Torsional stiffness can be normalized by comparing it to another set of characteristic

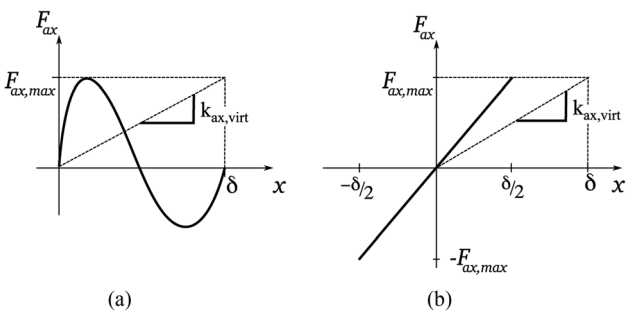

(a) (b)

Fig. 6 Illustration of the virtual axial stiffness for (*a*) a bistable mechanism and (*b*) linear mechanism

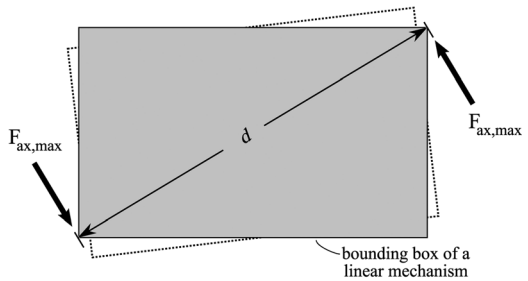

Fig. 7 The normalized torsional stiffness can be interpreted as normalized by a characteristic torque as illustrated here with a theoretical mechanism with a force of magnitude $F_{ax,max}$ and couple moment arm of length d

values. Using a product of actuation force, $F_{ax,max}$, and the mechanism size, d, the normalized torsional stiffness is defined as

$$k^*_{tors} = \frac{k_{tors,min}}{F_{ax,max} \cdot d} \tag{5}$$

This can be interpreted as normalization by a characteristic torque, T_{char}, consisting of a force of magnitude $F_{ax,max}$ and couple moment arm equal to the mechanism size, d, defined as

$$T_{char} = F_{ax,max} \cdot d \tag{6}$$

This interpretation suggests that the metric produces the inverse of the angle (in radians, which is also dimensionless) that results from the application of the characteristic torque as illustrated in Fig. 7. Thus it is nondimensional and effectively normalizes the torsional stiffness of the mechanism.

The final form of the travel and stiffness metrics are summarized in Table 2.

Table 2 Summary of the LLCM performance metrics

	Metric Formula	Normalizing Comparison
Travel	$\delta^* = \frac{\delta}{\sqrt{w^2+l^2}}$	Total displacement: device footprint
Transverse stiffness	$k^*_{transv} = \frac{k_{transv,min}}{F_{ax,max}/\delta}$	Minimum transverse stiffness: virtual axial stiffness
Torsional stiffness	$k^*_{tors} = \frac{k_{tors,min}}{F_{ax,max} \cdot d}$	Minimum torsional stiffness: characteristic torque

4 Demonstration of the Metrics: FEA Comparison

In this section, the performance of selected mechanism designs are evaluated to demonstrate the computation of the metrics and their usefulness in design. The compliant mechanisms that were simulated included the folded beam [4], the CT joint [3], and the X-Bob [6], illustrated in Fig. 8.

4.1 LLCM Devices

4.1.1 Folded Beam Suspension. The folded beam suspension is a popular design because of its simplicity and predictability. The basis of the device is a parallel-guiding mechanism, a linkage where the legs opposite each other are the same length. To form a folded-beam suspension, a number of parallel-guiding mechanisms are combined in series and parallel as shown in Fig. 8(*a*). A microscope image of two micro-scale folded beam suspensions in parallel is shown in Fig. 11(*a*). This combination of parallel-guiding devices constrains the shuttle to approximate straight-line motion.

4.1.2 CT Joint. The compliant translational (CT) joint was proposed as an improvement of a leaf spring joint, increasing the range of motion and also improving the transverse stiffness. The mechanism is composed of compliant members constrained by the parallel arrangement of two identical plates. The joint can be modeled as a parallel four-bar mechanism and allows only pure translational motion [3]. The CT joint is illustrated in Fig. 8(*b*); the dashed lines show the deflected state of the mechanism with the left plate being considered ground.

4.1.3 X-Bob Suspension. The X-Bob, as illustrated in Fig. 8(*c*), is another example of a planar, large-displacement device consisting of a center shuttle on a compliant suspension [6]. The X-Bob configuration has proven to be effective for micro-systems; a micro machined version is shown in the microscope image of Fig. 11(*b*).

4.2 Simulations and Comparisons. The simulations used a commercial finite element method capable of nonlinear analysis (ANSYS) with 2D beam elements (BEAM3). Each simulation represented one of the three basic designs in the preceding text with a variation in only the in-plane thickness of the flexures. Details on the simulations and the dimensions of these configurations are included in Ref. [14]. These examples serve to demonstrate the metrics, but they are not a comprehensive evaluation of the potential performance of the devices for all possible configurations. A complete comparison of the devices would simulate configurations that explore all the variations in geometry and potential material properties across the design space for the three designs.

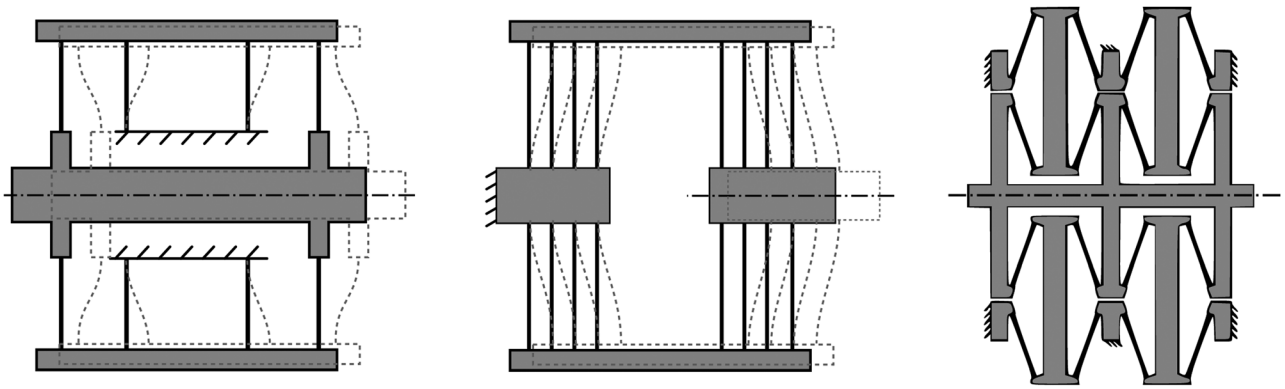

Fig. 8 Three mechanisms used in the case study: (*a*) folded beam [4]; (*b*) CT joint [3]; (*c*) XBob [6]

Performance was evaluated at successive steps along the axis until the maximum stress in a flexure reached the yield strength. This was accomplished using the following procedure:

1. For step i, displace the shuttle axially to $x = x_i$ and record the resulting axial force, $F_{ax}(x_i)$.
2. Holding the axial position constant, displace the device in the transverse direction (Δy) and record the associated transverse force, $F_{transv}(x_i)$. Calculate the transverse stiffness as the transverse force divided by the perturbation, Δy:

$$k_{transv}(x_i) = \frac{F_{transv}(x_i)}{\Delta y} \tag{7}$$

3. Continuing to hold the axial position constant, allow the shuttle to return from its transverse displacement, and rotate the shuttle to a small angle ($\Delta\theta$) and record the resulting torque, $T(x_i)$. Calculate the torsional stiffness as the torque divided by the perturbation angle, $\Delta\theta$

$$k_{tors}(x_i) = \frac{T(x_i)}{\Delta\theta} \tag{8}$$

4. Determine the total deflection, δ, from physical limitations (e.g., stress limitations or interference of components) or other limits on travel imposed by the designer.
5. Calculate the normalized stiffnesses k^*_{transv} and k^*_{tors} and displacement δ^* using equations (2), (3), and (5). These values determine the performance of one simulation (one of the three mechanisms with a specified flexure thickness) and is represented by a single point on each graph.

The resulting evaluations are shown in Figs. 9 and 10. Each data point represents an individual simulation. With more simulations that explore variations in the designs, it could be possible to produce approximate performance regions for each mechanism type (e.g., a cloud of points that describe the folded beam). These clouds could then be used to compare performance for the mechanism types.

Of the designs simulated in this study, the design with the longest travel is a CT joint with very thin flexures. However, this design also has low off-axis stiffness in both the transverse and torsional cases. The X-Bob designs possess high transverse stiffness, while the designs of the folded beam exhibit high torsional stiffness. In general, all three concepts show an increase in travel due to the thinning of the flexures.

These examples illustrate the trade-offs made in designing LLCMs. Some improvements in off-axis stiffness may be made

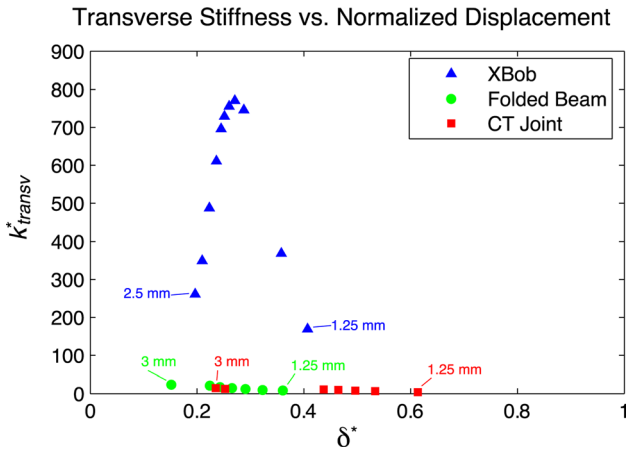

Fig. 9 Demonstration of the use of the transverse stiffness metric with several sample configurations simulating a variation in in-plane thickness for the three concepts

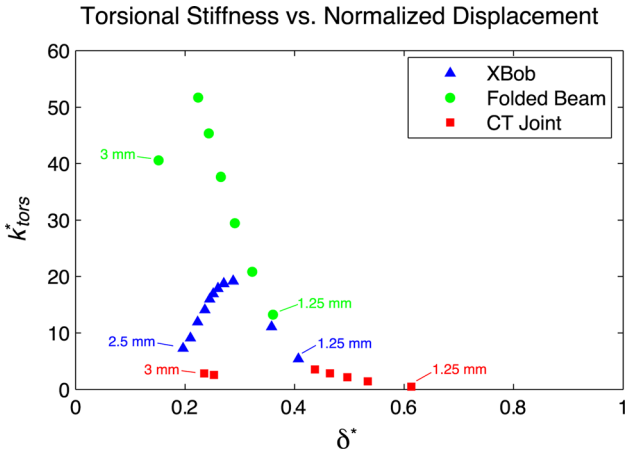

Fig. 10 Demonstration of the use of the torsional stiffness metric with several sample configurations simulating a variation in in-plane thickness for the three concepts

by changing the in-plane thickness as in the case of the X-Bob in these simulations. However, attempts to increase the off-axis stiffness by increasing the thickness of the flexures often results in higher axial resistance. The increase in axial stiffness counteracts the improvement in off-axis stiffness and results in little change in the stiffness ratio. Likewise, attempts to decrease axial resistance through the use of thinner flexures results in lower off-axis stiffness and again, little change in the stiffness ratio.

This suggests that while some small improvements can be made by altering the flexures, the largest opportunities are at the conceptual level to make significant increases in stiffness. It would be valuable to have new concepts that obtain consistently high off-axis stiffness as many designs displayed a dramatic decrease in off-axis stiffness when displaced from the home position,

The scope of this work was limited to addressing off-axis stiffness for in-plane forces without addressing out-of-plane moments or out-of-plane forces. Future work could extend or modify these metrics to apply to off-axis stiffness in other directions.

5 Demonstration of Metrics: Example Implementation

Microelectromechanical systems (MEMS) are particularly sensitive to size and transverse stiffness. The relatively high cost of wafer real estate often puts footprint size at a premium during the design process. However, because of the small scale, precision is also key, and motion in unwanted directions can prohibit the device from functioning properly. As several methods of achieving large displacements exist, the metrics can be used to compare the devices and determine which is the best fit for a given application.

In this section, the metrics were used to characterize and compare four LLCM MEMS devices: a folded beam suspension, large and small X-Bob suspensions, and a double X-Bob suspension. All four designs consist of a center shuttle attached to a compliant suspension. With the exception of the small X-Bob, all were designed to allow 250 μm unidirectional displacement (500 μm total) with a reasonable safety factor. The small X-Bob was designed for 125 μm unidirectional displacement. A description of each of the devices, and the calculation of their metrics follow. The metrics were then used as the objectives for an optimization of the X-Bob design.

5.1 Travel Metrics. The dimensions of the rectangular bounding box for this folded beam suspension are $w = 912$ μm and $l = 1880$ μm. The travel metric can be calculated from Eq. (1) as

$$\delta^* = \frac{2 * 250}{\sqrt{912^2 + 1880^2}} = 0.239 \tag{9}$$

Table 3 X-Bob travel metric information

Variable	Large	Small
δ	250 μm	125 μm
W	1480 μm	890 μm
L	1850 μm	1675 μm
δ^*	0.211	0.132

Two variations of the X-Bob were tested in this study, a large and small design. The relative link lengths, which govern the stress states of the compliant suspension, are different in each of the designs, giving different values of the metrics. The small X-Bob suspension was designed for 125 μm of uniaxial displacement, and has bounding box dimensions of $w = 890$ μm and $l = 1675$ μm. The large X-Bob suspension was designed for 250 μm of uniaxial displacement with bounding box dimensions of $W = 1480$ μm and $L = 1850$ μm. From this information, the travel metric can be calculated for both designs. The designed displacement, bounding box dimensions, and values of the travel metrics are listed in Table 3.

The double X-Bob is a variation of the X-Bob design. This particular device combines two small X-Bob suspensions in series by layering them one directly on top of the other, in different structural layers of polysilicon. In the home position, this double X-Bob looks identical to the small X-Bob suspension as shown in Fig. 11(*b*). The double X-Bob extended is shown in Fig. 11(*c*).

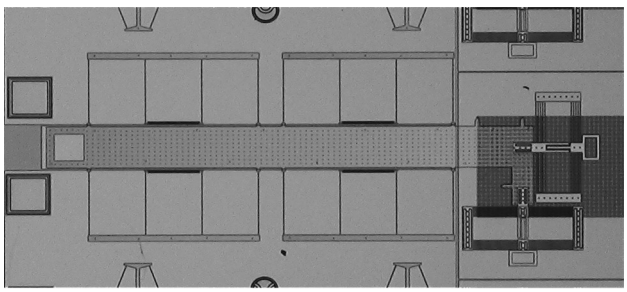

(a)

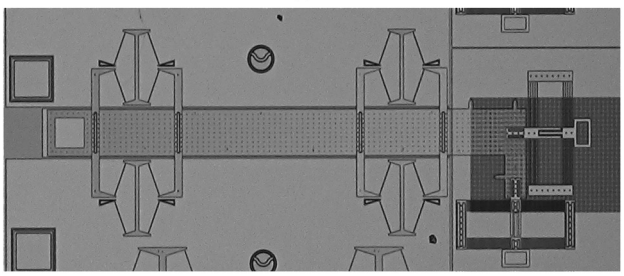

(b)

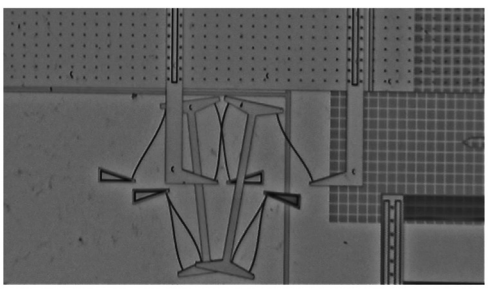

(c)

Fig. 11 Micrographs of (*a*) a folded-beam suspension large-displacement device, (*b*) an X-Bob suspension large-displacement device, and (*c*) a double X-Bob suspension

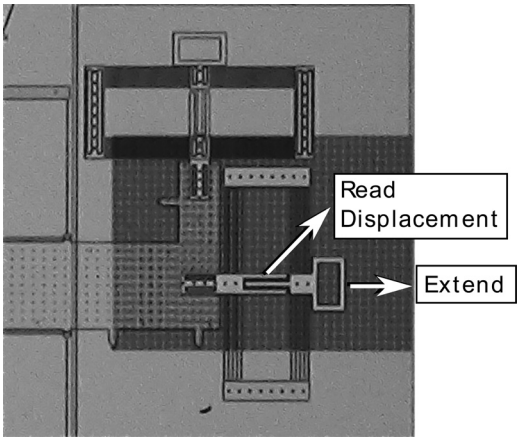

Fig. 12 Force gauges for measuring axial and transverse force-deflection relationships

This device has the same bounding box parameters as the small X-Bob, which are shown in Table 3. The travel metric is

$$\delta^* = \frac{2 * 250}{\sqrt{890^2 + 1675^2}} = 0.264 \tag{10}$$

5.2 Transverse Stiffness Metrics. Calculating the transverse stiffness metric requires the force-deflection relationship for each device in the axial and transverse directions. To measure the force-deflection relationships for the given devices, surface micromachined force gauges [15] were fabricated as part of each device. The force gauges are on one end of the shuttle and allow the force to be measured in both the axial and off-axis directions. The force gauges are shown on the right sides of the devices in Figs. 11(*a*) and 11(*b*). The axial force deflection relationships were realized by extending the shuttle using a microprobe and recording the displacement of the force gauge as shown in Fig. 12. The gauge displacement can then be translated into a force. The results of the test were plotted, and the resulting force-displacement curves are shown in Fig. 13.

Because the axial stiffness can be a function of x, the calculation of k^*_{trans} uses the virtual axial stiffness. Because the mechanisms here exhibited linear force displacement relationships, the virtual axial stiffness can also be calculated as half of the axial spring constant (refer to Eq. (4) and the discussion that follows). The force deflection data for each device can be fit with a linear model, and the relationship for the slope of the line can be recognized as the axial spring constant, k_{axial}. The virtual axial stiffness for each device is listed in Table 4.

The off-axis stiffness was tested using a method similar to that used for testing the axial force-deflection relationship. Using microprobes to manipulate the device, the shuttle was extended

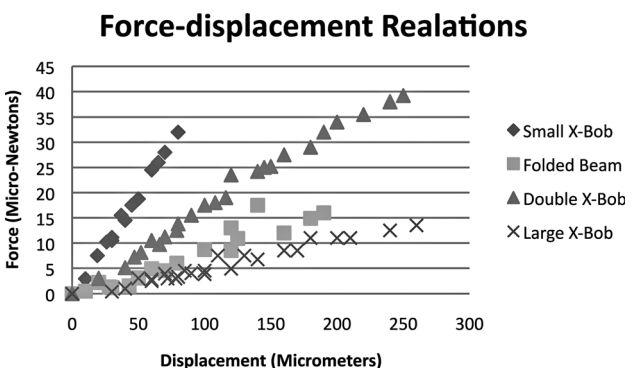

Fig. 13 Force-deflection relationships for 4 micro-devices

Table 4 Comparison of transverse stiffness values

Configuration	$k_{ax,\ virt}$	$k_{trans,\ min}$	k^*_{trans}
Folded beam	0.046	1.21	26.3
Small X-Bob	0.196	10.03	51.2
Large X-Bob	0.028	1.83	65
Double X-Bob	0.082	2.83	34.5

Table 5 Comparison of metrics

Configuration	δ^*	k^*_{trans}
Folded Beam	0.239	26.3
Small X-Bob	0.132	51.1
Large X-Bob	0.211	65
Double X-Bob	0.264	34.5
Optimized X-Bob	0.226	80.6

from one end of the shuttle, while a transverse force was applied on the opposite end. Displacements were assigned a random order, and at each displacement an off-axis force was applied to the shuttle via the force gauge. Shuttle displacements were recorded for every 5 μm of force gauge displacement. The force-gauge displacements were translated into forces and used to create 3-D surfaces representing the off-axis displacement for a given shuttle displacement and off-axis force. The 3-D surface created for the small X-Bob is shown in Fig. 14; similar plots were created for the other device configurations.

The minimum value for the transverse spring constant was used to calculate the transverse stiffness, k^*_{trans}, for each device; as expected, the minimum k^*_{trans}, was found at the maximum extension, and maximum applied force. Table 4 lists the results for the virtual axial stiffness, transverse stiffness, and the transverse stiffness metric.

6 Demonstration Of Metrics: Design Example

The results of the testing and characterization indicate that the X-Bob configurations provide high transverse stiffness, while the folded-beam and double X-Bob suspensions are more space conservative for a given displacement. As an example of using the metrics in designs, consider an application of interest where transverse stiffness is the most critical parameter for device performance.

The resulting design must have the following characteristics: it must be able to achieve a displacement of 250 μm, and the value of the travel metric must be at least as large as that of the large X-Bob. The value of the transverse-stiffness metric is to be maximized.

A genetic algorithm was chosen as the optimization routine. It was programmed (in Matlab) and linked to commercial FEA software (ANSYS) [16], which was utilized to find the force-deflection relationships in the axial and transverse directions as well as the maximum stress in the device. Penalties were applied if the design travel metric was less than 0.211 if the maximum stress exceeded 1 GPa or if the geometry was not feasible for planar fabrication. The details of this optimization have been published previously [17].

The simulated values of the resulting design show a marginally improved travel metric, while the transverse-stiffness metric, the objective of the optimization, improved by 24%. Table 5 lists the metric values for the new design and values for each of the previous devices. Figure 15 shows a microscope image of both the large X-Bob design (Fig. 15(*a*)), and the optimized design (Fig. (*b*)). This example demonstrates the value of using the new metrics in design.

7 Conclusions

The metrics developed in this paper provide an improved approach for evaluating the performance of LLCMs, laying the groundwork for designers to develop mechanisms with improved performance. They show that design improvements can be made by altering the flexures, but the largest opportunities for increased performance are at the conceptual level. The metrics were demonstrated in the evaluation of several LLCMs and the use of metrics in design was illustrated by the design of a LLCM MEMS device.

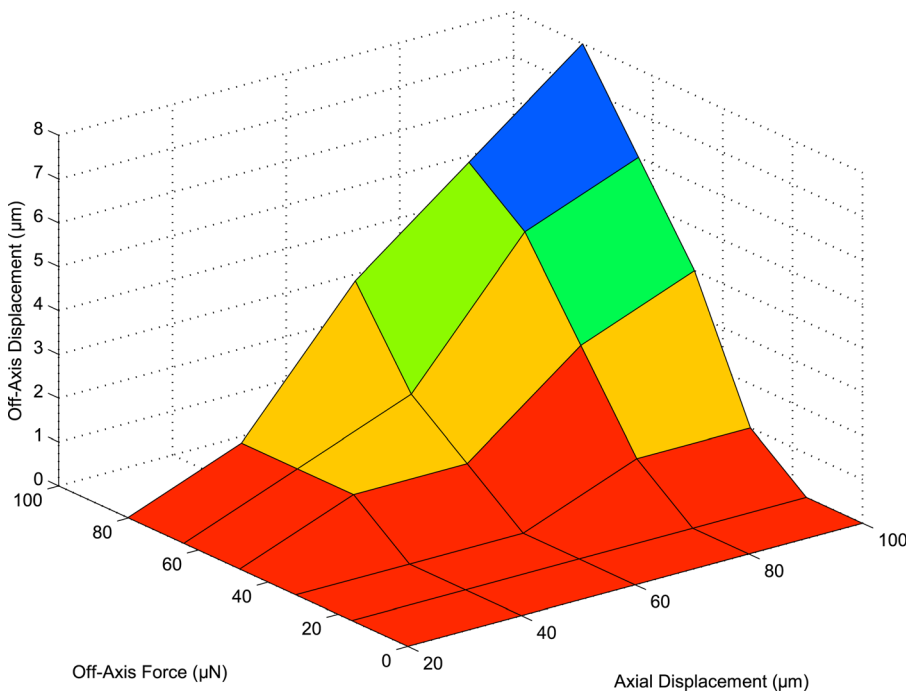

Fig. 14 Transverse-displacement 3D plot for small X-Bob suspension, similar plots were created for all of the device configurations

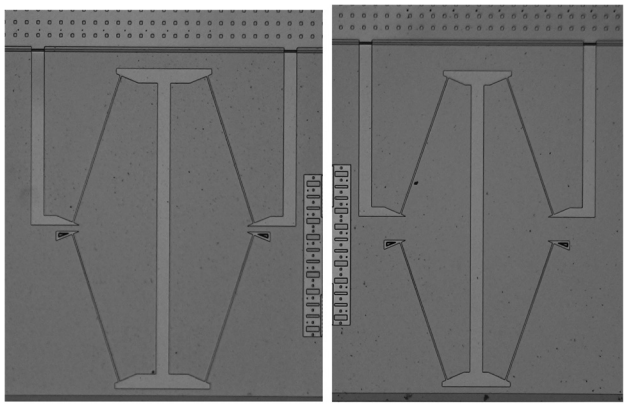

(a) (b)

Fig. 15 Microscope images of (*a*) a large X-Bob design and (*b*) an optimized X-Bob design

The metrics provide tools for the development and evaluation of new compliant linear mechanisms that can overcome the current displacement-stiffness trade-offs to yield much longer travel capabilities. The main outcomes of performance for LLCMs are increased travel, increased transverse stiffness, increased torsional stiffness, decreased axial force, and decreased mechanism size. It was also shown that many previous linear mechanisms have low off-axis stiffness due to a decrease in off-axis stiffness when displaced from the home position. By applying the metrics to designs that span the design space of a given concept, the metrics create a performance region for each concept. This evaluation approach can be used to compare the performance of different LLCM concepts.

Testing has been done and metrics calculated for the comparison of four LLCM MEMS devices. Planar X-Bob suspensions showed high transverse stiffness while the folded-beam and double X-Bob suspensions were found to have large displacement relative to device footprint. Optimizing the design for the planar X-Bob suspension yielded a simulated configuration with improved displacement for a given footprint, while increasing the value of the transverse stiffness metric by 24%. This optimized design has significant implications for applications that require high off-axis stiffness for the functionality of the device.

The metrics described here lay the foundation for improved large-displacement linear-motion mechanism designs. These improved designs impact many related applications including handheld electronics, optical alignment, micro-grasping, and optical switching.

Acknowledgment

The authors gratefully acknowledge the support of Nokia Research Center, Block MEMS, LLC, and the Army Research Office (subcontract through Block MEMS, LLC).

References

[1] Howell, L. L., 2001. *Compliant Mechanisms* (Wiley-Interscience, New York, 2001).
[2] Halverson, P., Howell, L. L., and Magleby, S. P., 2010, "Tension-Based Multi-Stable Compliant Rolling-Contact Elements". Mechan. Mach. Theory, **45**(2), pp. 147–156.
[3] Trease, B. P., Moon, Y.-M., and Kota, S., 2005, "Design of Large-Displacement Compliant Joints". ASME J. Mechan. Des., **127**(4), pp. 788–798.
[4] Cannon, B. R., Lillian, T. D., Magleby, S. P., Howell, L. L., and Linford, M. R., 2005, "A Compliant End-Effector for Microscribing," Precision Eng., **29**(1), pp. 86–94.
[5] Saggere, L., Kota, S., and Crary, S., 1994. "New Design for Suspension of Linear Microactuators," ASME Dynam. Syst. Control Div. **55**(2), pp. 671–675.
[6] Hubbard, N. B., Wittwer, J. W., Kennedy, J. A. L., Wilcox, D., and Howell, L. L., 2004, "A Novel Fully Compliant Planar Linear-Motion Mechanism," *Proceedings of the 2004 ASME Design Engineering Technical Conferences* (DETC2004-57008), Salt Lake City, UT.
[7] Gomm, T., Howell, L. L., and Selfridge, R., 2002, "In-Plane Linear Displacement Bistable Microrelay," J. Micromechan. Microeng., **12**(3), pp. 257–264.
[8] Cazottes, P., Fernandes, A., Pouget, J., and Hafez, M., 2009. "Bistable Buckled Beam: Modeling of Actuating Force and Experimental Validations," ASME J. Mechan. Des., **131**(10), October, 101001-1–101001-10.
[9] Todd, B., Jensen, B. D., Schultz, S. M., and Hawkins, A. R., 2010, "Design and Testing of a Thin-Flexure Bistable Mechanism Suitable for Stamping From Metal Sheets," ASME J. Mechan. Des., **132**(7), pp. 071011-1–071011-7.
[10] Masters, N. D., and Howell, L. L., 2003, "A Self-Retracting Fully Compliant Bistable Micromechanism," J. Microelectromechan. Syst., **12**(3), June, pp. 273–280.
[11] Wilcox, D. L., and Howell, L. L., 2005, "Double-Tensural Bistable Mechanisms (DTBM) With On-Chip Actuation and Spring-Like Post-Bistable Behavior," *Proceedings of the 2005 ASME Design Engineering Technical Conferences* (DETC2005-84697), Long Beach, CA.
[12] Vehar, C., Kota, S., and Dennis, R., 2004, "Closed-Loop Tape Springs As Fully Compliant Mechanisms -Preliminary Investigations," *Proceedings of the 2004 ASME Design Engineering Technical Conferences 2B* (DETC2004-57403), Salt Lake City, UT, pp. 1023–1032.
[13] Guerinot, A. E., Magleby, S. P., Howell, L. L., and Todd, R. H., 2005, "Compliant Joint Design Principles for High Compressive Load Situations," ASME J. Mechan. Des., **127**, pp. 774–781.
[14] Mackay, A. B., 2007, "Large-Displacement Linear-Motion Compliant Mechanisms," Master's thesis, Brigham Young University, Provo, UT.
[15] Wittwer, J. W., Gomm, T., and Howell, L. L., 2002, "Surface Micromachined Force Gauges: Uncertainty and Reliability," J. Micromechan. Microeng., **12**(1), pp. 13–20.
[16] Roman, G. A., and Wiens, G. J., 2007, "MEMS Optical Force Sensor Enhancement via Compliant Mechanism," *Proceedings of the ASME 2007 International Design Engineering Technical Conferences* (DETC2007-35345), Las Vegas, NV.
[17] Smith, D. G., Larsen, G. T., and Howell, L. L., 2009, "Design Optimization of a Linear-Motion Large-Displacement Micro Mechanism for High Off-Axis Stiffness," *Proceedings of the ASME 2009 International Design Engineering Technical Conferences* (DETC2009-87301), San Diego, CA.